Comparison of Static and Dynamic ^{18}F-FDG PET/CT for Quantification of Pulmonary Inflammation in Acute Lung Injury

Anja Braune[1,2], Frank Hofheinz[3], Thomas Bluth[1], Thomas Kiss[1], Jakob Wittenstein[1], Martin Scharffenberg[1], Jörg Kotzerke*[2], and Marcelo Gama de Abreu*[1]

[1]*Pulmonary Engineering Group, Department of Anesthesiology and Intensive Care Medicine, University Hospital Carl Gustav Carus at the Technische Universität Dresden, Dresden, Germany;* [2]*Department of Nuclear Medicine, University Hospital Carl Gustav Carus at the Technische Universität Dresden, Dresden, Germany; and* [3]*PET Center, Institute of Radiopharmaceutical Cancer Research, Helmholtz-Zentrum Dresden-Rossendorf, Dresden, Germany*

PET imaging with ^{18}F-FDG followed by mathematic modeling of the pulmonary uptake rate (K_i) is the gold standard for assessment of pulmonary inflammation in experimental studies of acute respiratory distress syndrome (ARDS). However, dynamic PET requires long imaging and allows the assessment of only 1 cranio-caudal field of view (~15 cm). We investigated whether static ^{18}F-FDG PET/CT and analysis of SUV or standardized uptake ratios (SUR_{stat}, uptake time–corrected ratio of ^{18}F-FDG concentration in lung tissue and blood plasma) might be an alternative to dynamic ^{18}F-FDG PET/CT and Patlak analysis for quantification of pulmonary inflammation in experimental ARDS. **Methods:** ARDS was induced by saline lung lavage followed by injurious mechanical ventilation in 14 anesthetized pigs (29.5–40.0 kg). PET/CT imaging sequences were acquired before and after 24 h of mechanical ventilation. K_i and the apparent volume of distribution were calculated from dynamic ^{18}F-FDG PET/CT scans using the Patlak analysis. Static ^{18}F-FDG PET/CT scans were obtained immediately after dynamic PET/CT and used for calculations of SUV and SUR_{stat}. Mean K_i values of the whole imaged field of view and of 5 ventro-dorsal lung regions were compared with corresponding SUV and SUR_{stat} values, respectively, by means of linear regression and concordance analysis. The variability of the ^{18}F-FDG concentration in blood plasma (arterial input function) was analyzed. **Results:** Both for the whole imaged field of view and ventro-dorsal subregions, K_i was linearly correlated with SUR_{stat} ($r^2 \geq 0.84$), whereas K_i–SUV correlations were worse ($r^2 \leq 0.75$). The arterial input function exhibited an essentially invariant shape across all animals and time points and can be described by an inverse power law. Compared with K_i, SUR_{stat} and SUV tracked the same direction of change in regional lung inflammation in 98.6% and 84.3% of measurements, respectively. **Conclusion:** The K_i–SUR_{stat} correlations were considerably stronger than the K_i–SUV correlations. The good K_i–SUR_{stat} correlations suggest that static ^{18}F-FDG PET/CT and SUR_{stat} analysis provides an alternative to dynamic ^{18}F-FDG PET/CT and Patlak analysis, allowing the assessment of inflammation of whole lungs, repeated measurements within the period of ^{18}F-FDG decay, and faster data acquisition.

Key Words: pulmonary inflammation; positron emission tomography; ^{18}F-FDG; tumor-to-blood standardized uptake ratio; standardized uptake value

J Nucl Med 2019; 60:1629–1634
DOI: 10.2967/jnumed.119.226597

Acute respiratory distress syndrome (ARDS) is an inflammatory condition of the lung and associated with high morbidity and mortality (*1*). Noninvasive in vivo measurement of the degree and distribution of pulmonary inflammation can improve understanding of this syndrome and the impact of mechanical ventilation. PET/CT imaging of the uptake rate (K_i) of ^{18}F-FDG is a valuable method to determine the pulmonary inflammatory response in ARDS. ^{18}F-FDG PET/CT measurements are based on the fact that pulmonary inflammation is associated with regionally increased accumulation of inflammatory cells, especially neutrophils, which have higher glucose metabolism than other pulmonary cells (*2,3*). The more pronounced regional uptake of ^{18}F-FDG and the associated higher radioactivity originating from a local inflamed region can therefore be used to assess the degree and distribution of lung inflammation in ARDS.

Dynamic ^{18}F-FDG PET/CT acquires time–activity data over a long period after ^{18}F-FDG injection (typically over 60–75 min). On mathematic modeling, these data allow the calculation of dynamic indices such as K_i. Such models take into account the transportation rates between blood and tissue compartments. However, dynamic PET requires long image acquisition and allows the assessment of only 1 cranio-caudal field of view (FOV), which usually captures approximately 15 cm and thus not the whole lung. The captured lung region has to be defined beforehand, when the degree and distribution of pulmonary inflammation are not yet known.

Static PET scanning of the decay rate of ^{18}F-FDG allows fast image acquisition and can cover an unlimited FOV, enabling acquisition of the whole lung. The SUV, a simple and widely used parameter for quantification of static PET scans, represents the mean activity concentration within a region of interest (ROI) normalized to the injected dose and body weight. However, SUVs strongly depend on the ^{18}F-FDG uptake of other organs and tissue, affecting the amount of ^{18}F-FDG in blood plasma available for uptake by lung tissue. This effect is of particular importance in

Received Feb. 7, 2019; revision accepted Apr. 24, 2019.
For correspondence or reprints contact: Anja Braune, Department of Nuclear Medicine, University Hospital Carl Gustav Carus, Fetscherstrasse 74, D-01307 Dresden, Germany.
E-mail: anja.braune@uniklinikum-dresden.de
*Contributed equally to this work.
Published online May 3, 2019.

the lung because of its much lower ^{18}F-FDG uptake than in other organs such as the kidney, heart, or brain (*4*) and has potentially caused a weak K_i–SUV correlation in dogs with lung injury (*2*), patients with liver metastases (*5*), and patients with non–small cell lung cancer (*6*). van den Hof et al. introduced the standardized uptake ratio (SUR), which is defined as tissue SUV normalized to the ^{18}F-FDG concentration in blood plasma available for influx into the tissue (*5*). Therefore, SUR takes into account the ^{18}F-FDG uptake of other bodily tissues and organs. In comparison to the dynamic index K_i, reflecting the ^{18}F-FDG uptake over time, static indices such as SUR reveal the amount of ^{18}F-FDG within a ROI at the time point of a static PET/CT scan.

In this study, we investigated whether SUV or SUR values derived from static PET scanning can be used as alternative to dynamic PET for quantification of regional lung inflammation in experimental ARDS.

MATERIALS AND METHODS

Experimental Protocol

The Institutional Animal Care and Welfare Committee and the Government of the State of Saxony, Germany, approved all animal procedures in accordance with federal law (AZ 24-9168.11-1/2013-53). The time course of interventions is shown in Figure 1. Briefly, after premedication (1 mg/kg midazolam, 10 mg/kg ketamine, 0.05 mg/kg atropine), 14 juvenile pigs (29.5–40.0 kg) were intravenously anesthetized (5–15 mg/kg ketamine, 0.3–1 mg/kg midazolam, both as bolus), paralyzed (3 mg/kg atracurium), orotracheally intubated, and mechanically ventilated (Evita XL; Dräger Medical AG) in the supine position. The lungs were ventilated in volume-controlled mode using the following settings: fraction of inspired oxygen, 1.0; tidal volume (V_T), 6 mL/kg; positive end-expiratory pressure, 10 cmH_2O; inspiratory-to-expiratory ratio, 1:1; constant airway flow, 35 L/min; and respiratory rate adjusted to achieve an arterial partial pressure of carbon dioxide between 35 and 45 mm Hg. During preparation, a crystalloid solution (E153; Serumwerk Bernburg AG) was infused intravenously at a rate of 10 mL/kg/h via a peripheral vein. A 8.5-French sheath was inserted in the right internal carotid artery, and a 7.5-French pulmonary artery catheter was advanced through another sheath placed in the right external jugular vein. The lungs were recruited with continuous positive airway pressure of 30 cmH_2O for 30 s followed by 15 min of stabilization. Experimental ARDS was induced using a double-hit model consisting of surfactant depletion (8 repetitive isotonic saline lung lavages alternating in prone and supine position) followed by injurious mechanical ventilation with high V_T (20 mL/kg) until the Horovitz index was less than 100 mm Hg for at least 30 min. After acquisition of baseline PET/CT imaging data, the animals were randomly assigned to mechanical ventilation with either variable volume-controlled ventilation with a mean V_T of 6 mL/kg and a coefficient of variation in V_T of 30% ($n = 7$) or volume-controlled ventilation with nonvariable V_T ($n = 7$). The fraction of inspired oxygen was titrated according to the low positive end-expiratory pressure table of the ARDS network, and the respiratory rate was adjusted to an arterial pH of more than 7.30. Further mechanical ventilation settings were as follows: inspiration–expiration ratio, 1:1; maximal plateau pressure, 30 cmH_2O and 45 cmH_2O for variable and nonvariable ventilation, respectively; and mean plateau pressure, 30 cmH_2O in the variable ventilation mode.

After randomization, the crystalloid solution infusion rate was changed to 4 mL/kg/h to maintain intravascular volume. Colloid solution (6% hydroxyethyl starch; Fresenius Kabi Deutschland GmbH) was administered as necessary to keep the hemoglobin concentration in the blood approximately constant. After 24 h of mechanical ventilation in variable or nonvariable ventilation mode, PET/CT imaging was repeated. Respiratory mechanics, gas exchange, and hemodynamics were assessed before and after induction of ARDS (injury), before the start of mechanical ventilation, and at 6 h intervals thereafter. At the end of the experiments, the animals were killed by intravenous injection of thiopental (2 g) followed by potassium chloride (1 M, 50 mL).

Lung Imaging Protocol and Image Processing

After induction of lung injury and before the start of 24 h of mechanical ventilation, as well as after 24 h of mechanical ventilation, imaging data were acquired according to the imaging protocol illustrated in Figure 1. Briefly, low-dose helical CT scans of the thorax were obtained during mechanical ventilation and used for attenuation correction of the following PET images (Biograph 16 HiRez PET/CT; Siemens). ^{18}F-FDG (198.6 ± 42.3 MBq) was injected intravenously over 60 s. Starting at the beginning of ^{18}F-FDG infusion, sequential PET frames (6 × 30 s, 7 × 60 s, 15 × 120 s, 1 × 300 s, and 3 × 600 s) were acquired over 75 min. The 15 cm cranio-caudal FOV of the dynamic PET scans was set above the diaphragmatic dome to reduce artifacts due to motion of the diaphragm. Pulmonary arterial blood was sampled during the time course of the dynamic PET scans (12 × 15 s, 4 × 30 s, 5 × 60 s, 11 × 300 s, and 75 min). The concentration of ^{18}F-FDG in 1 mL of blood plasma was measured in a γ-counter cross-calibrated with the PET scanner. Immediately after dynamic PET and 77–81 min after ^{18}F-FDG injection, static ^{18}F-FDG PET/CT scans were obtained at 3 bed positions assessing the whole lung.

Attenuation-correction CT scans were reconstructed with 2.0 mm slice thickness, yielding matrices with 512 × 512 pixels (1.37 × 1.37 mm). Static and dynamic PET scans were reconstructed with 2.0 mm slice thickness, yielding matrices with 168 × 168 pixels (2.03 × 2.03 mm). The reconstruction was performed iteratively (ordered-subset expectation maximization, 6 iterations, 4 subsets, 5 mm Gauss postfiltering) with correction for scatter and attenuation.

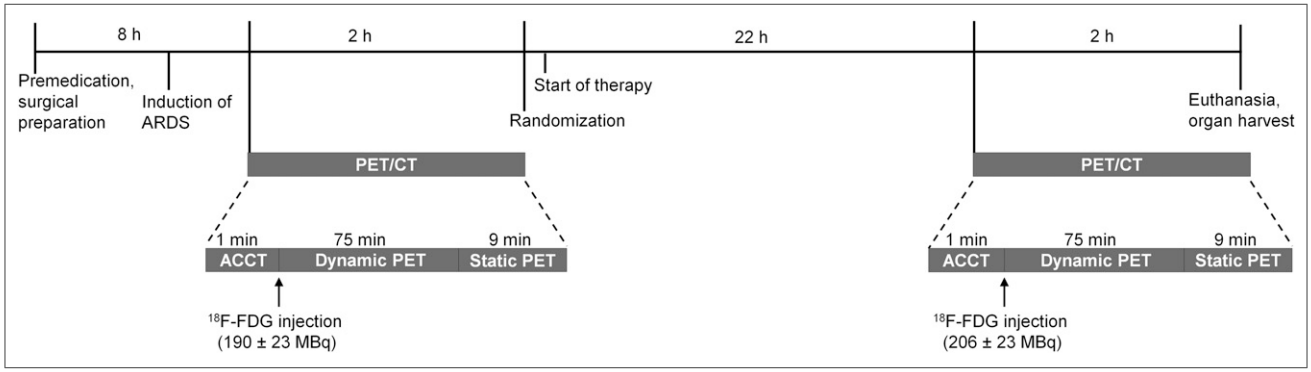

FIGURE 1. Time course of interventions. ACCT = CT-based attenuation correction.

Analysis of Blood Plasma Samples

For each animal and imaging sequence, the activity measurements of ^{18}F-FDG in blood plasma were interpolated to the mean frame time points of the dynamic PET scans, giving a subject-specific arterial input function ($C_p(t)$). For each animal and time point, an inverse-power law (Eq. 1) was fitted to the input function using the data at $t \geq 10$ min after ^{18}F-FDG injection:

$$C_p(t) = A \times t^{-b}. \quad \text{Eq. 1}$$

The resulting input function was extrapolated to the time after injection of the respective static PET scan. The extrapolated C_p values were used to compute the SUR of the static PET scans, for which no blood samples were available.

To validate whether Equation 1 can be used to adequately describe the input function, the time course of C_p was normalized to its mean value over the period of the dynamic PET scan to account for differing amounts of injected ^{18}F-FDG and for differing body weights (blood volume). The time-averaged C_p was compared between imaging sequences and animals by graphical illustration and by fitting Equation 1 to the time-averaged C_p data at $t > 3$ min and $t \geq 10$ min.

Image Analysis

Attenuation-correction CT scans and static PET scans were coregistered to the dynamic PET scans. Segmentation of the lung was performed on coregistered attenuation-correction CT scans to define ROIs, from which major airways and vessels were excluded. The acquired 15 cm cranio-caudal lung fields of view of the dynamic PET scans were divided into 5 isogravimetric subregions reaching from ventral to dorsal. The ROIs were applied to dynamic and static PET scans and were used to compute the corresponding concentration of ^{18}F-FDG in lung tissue (C_{PET}).

^{18}F-FDG K_i and the apparent distribution volume of ^{18}F-FDG in blood plasma as a fraction of tissue volume (V_{dist}) were derived from the Patlak graphical analysis of the dynamic PET frames acquired 10–75 min after ^{18}F-FDG injection using the following equation:

$$\frac{C_{PET}(t)}{C_p(t)} = K_i \times \theta(t) + V_{dist} \quad \text{with} \quad \theta(t) = \frac{\int_0^t C_p(\tau) \times d\tau}{C_p(t)}, \quad \text{Eq. 2}$$

where $\theta(t)$ is the so-called Patlak time and τ is the integration variable. K_i and V_{dist} were averaged for each ROI and for the whole FOV.

SUV was calculated from static PET scans as:

$$SUV(T) = \frac{C_{PET}(T)}{\text{injected dose/body weight}}. \quad \text{Eq. 3}$$

SUR was computed for the data of the dynamic PET scans acquired 40–75 min after injection (SUR_{dyn}) and the static PET scans (SUR_{stat}) as the uptake time–corrected ratio of tissue concentration and blood concentration, as previously described (*7*):

$$SUR(T_0) = \frac{T_0}{T} \times \frac{C_{PET}(T)}{C_p(T)}, \quad \text{Eq. 4}$$

where T is the actual scan time after injection and T_0 is the chosen standard scan time to which SURs are normalized. By definition, the uptake time of SUR_{dyn} is the same for all measurements; therefore, $T_0 = T$ was chosen (i.e., no scan time correction). The mean frame time point of the static PET scans ranged from 80.0 to 83.4 min. The mean value of the scan times was chosen as reference time $T_0 = 81.0$ min after injection. Mean values of SUV and SUR were calculated for the same ROIs as used for the Patlak analysis (thus covering only the 15 cm cranio-caudal FOV) and for the whole FOV.

For PET measurements before and after 24 h of mechanical ventilation, respectively, K_i–SUV, K_i–SUR_{stat}, and K_i–SUR_{dyn} correlations were investigated by means of linear regression and comparison of the coefficients of determination (r^2) for regional values and the whole FOV.

The ability of static PET scanning and SUV and SUR_{stat} analysis, respectively, to track the direction of change in regional lung inflammation induced by 24 h of mechanical ventilation and determined by dynamic PET scanning and Patlak K_i analysis was assessed by concordance analysis and calculation of the Cohen κ.

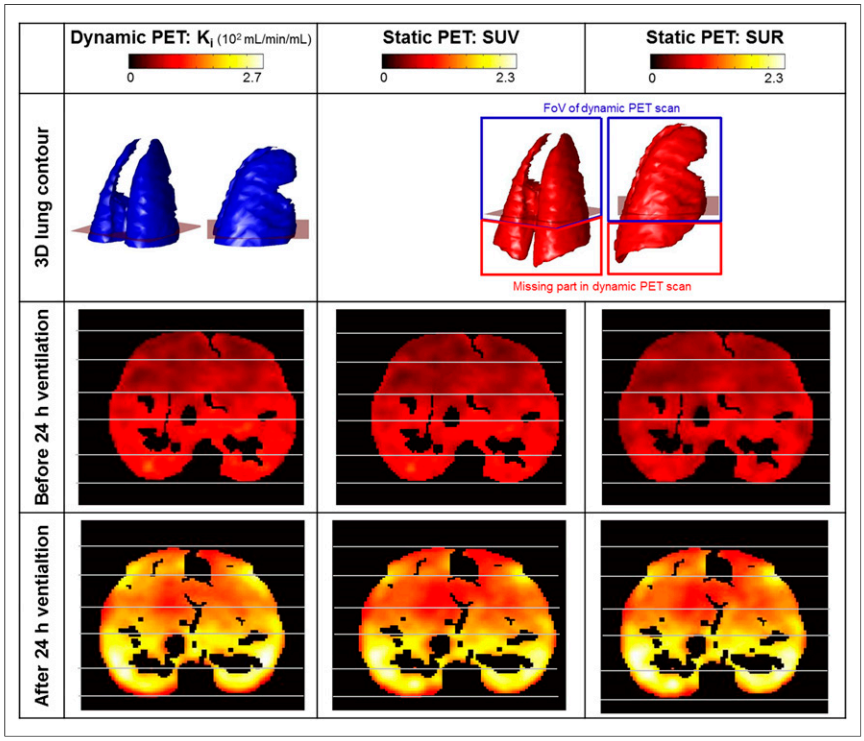

FIGURE 2. Three-dimensional (3D) lung contour and 2-dimensional (2D) transversal slices of 1 representative animal obtained before and after 24 h of mechanical ventilation. ^{18}F-FDG K_i was derived by dynamic PET/CT, whereas SUV and SUR_{stat} were derived from static PET/CT. Location of 2D transversal slices is shown in 3D contours. Caudal lung regions that were not assessed by dynamic PET scan because of its limited FOV are highlighted in 3D contours.

Statistics

A sample size calculation was not performed. Data are presented as mean and SD if not stated otherwise. Wilcoxon tests were used for comparisons between measurement time points. For the analysis of hemodynamics, gas exchange, and lung mechanics, differences between and within groups (group effect, time × group effect) were tested with general linear model statistics. Differences between groups at the time of injury and at the final assessment were tested with Mann–Whitney *U* tests. Significance was accepted at a *P* value of less than 0.05. Statistical analysis was performed with SPSS (version 23; IBM).

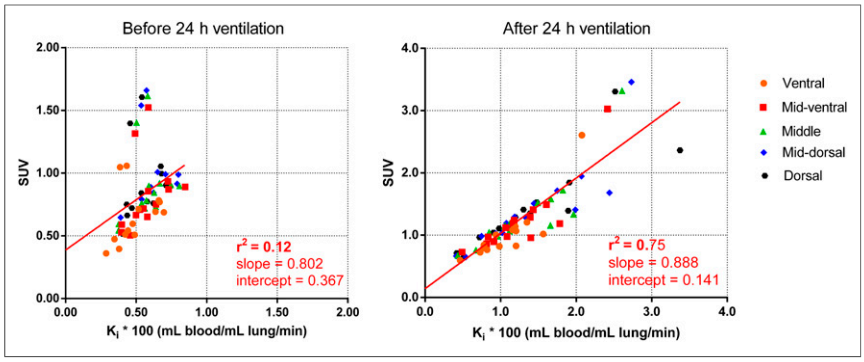

FIGURE 3. K_i–SUV correlation obtained from PET/CT imaging data acquired before and after 24 h of mechanical ventilation and divided into 5 isogravimetric ventral (non–gravitation-dependent)–dorsal (gravitation-dependent) regions. Red lines represent linear regression lines. Note differing axis scales, for which slope and intercept are specified.

RESULTS

Hemodynamics, gas exchange, and lung mechanics data are shown in Supplemental Table 1 (supplemental materials are available at http://jnm.snmjournals.org). There was no group effect or time × group effect for any of the variables. Variables regarding hemodynamics and gas exchange were comparable between groups at the time of injury and at the final assessment (Supplemental Table 1).

Maps of pulmonary inflammation of a representative animal obtained by static and dynamic ^{18}F-FDG PET/CT scanning before and after 24 h of mechanical ventilation are shown in Figure 2. The 15 cm cranio-caudal FOV assessed by dynamic PET scanning covered 76.43% ± 9.61% of the volume of the whole lung and 65.58% ± 5.96% of the cranio-caudal lung expansion (Fig. 2). In comparison, static PET scans covered the whole lung. Static PET scans were acquired 81.0 ± 0.81 min after injection of ^{18}F-FDG and 11.0 ± 0.81 min after the mean time point of the last dynamic PET frame. Dynamic PET scans were acquired over 75 min, whereas acquisition of static PET scans lasted 9 min.

The 24 h period of mechanical ventilation was associated with a 127.2% ± 79.4%, 63.2% ± 68.0%, and 99.2% ± 76.5% increase in regional K_i, SUV, and SUR_{stat}, respectively (Figs. 3 and 4).

Before the 24 h ventilation period, the K_i–SUV correlation was weak, both for the whole FOV (r^2 = 0.08) and for the 5 ventro-dorsal ROIs (r^2 = 0.12, Fig. 3). The K_i–SUV correlation was stronger after 24 h of mechanical ventilation (whole FOV, r^2 = 0.73; 5 ventro-dorsal ROIs, r^2 = 0.75; Fig. 3). The K_i–SUV correlation was worse than the K_i–SUR_{stat} correlation (Figs. 3 and 4). Before and after 24 h of mechanical ventilation, K_i and SUR_{stat} were correlated both for the whole FOV (r^2 = 0.94 and 0.97, respectively; Supplemental Fig. 2) and for the 5 ventro-dorsal ROIs (r^2 = 0.84 and 0.97, respectively; Fig. 4). The K_i–SUR_{stat} correlation was higher after 24 h of mechanical ventilation, when inflammation increased substantially (Fig. 4).

Static PET scanning and SUR_{stat} and SUV analysis, respectively, were able to predict the direction of change in regional lung inflammation, as determined by dynamic PET and K_i analysis, in 98.6% and 84.3% of measurements (Fig. 5). The smallest change in K_i that was still detected as an increase in SUR_{stat} was 0.0006 mL/mL/min (Fig. 5). The agreement between changes in K_i and SUR_{stat} induced by 24 h of mechanical ventilation was good (Cohen κ, 0.66), whereas there was no agreement between changes in K_i and SUV (Cohen κ, −0.027).

Figure 6A shows the time course of the time-averaged C_p of all animals and both imaging sequences. The very small SD of C_p at mean frame time points beyond $t > 3$ min after ^{18}F-FDG injection and the excellent agreement of the interpolation function with time-averaged C_p (r^2 = 0.99) illustrates the small inter- and intrasubject variability of the mean normalized activity of ^{18}F-FDG in blood plasma, despite much higher inflammatory values after 24 h of mechanical ventilation. The low variability is especially true at late time points, which are the relevant ones for the K_i–SUR_{stat} correlation. As a consequence, θ featured a relatively low inter- and intrasubject variability (low relative SD, e.g., at t = 70 min: 8.7%) and was linearly correlated with time for each animal and measurement time point (Fig. 6B).

V_{dist} was lowest in ventral regions and increased along the gravitational gradient at both imaging time points (Fig. 7). The 24 h period of mechanical ventilation was associated with a 23.2% ± 25.0% increase in mean regional V_{dist}.

K_i and SUR_{dyn} were strongly correlated (r^2 = 0.78 before and 0.97 after 24 h of mechanical ventilation, Supplemental Fig. 3). Although the K_i–SUR_{dyn} correlation was similar to the K_i–SUR_{stat} correlation for higher inflammatory values obtained after 24 h of mechanical ventilation, K_i–SUR_{dyn} was worse than K_i–SUR_{stat} before 24 h of mechanical ventilation (lower r^2, Supplemental Fig. 3).

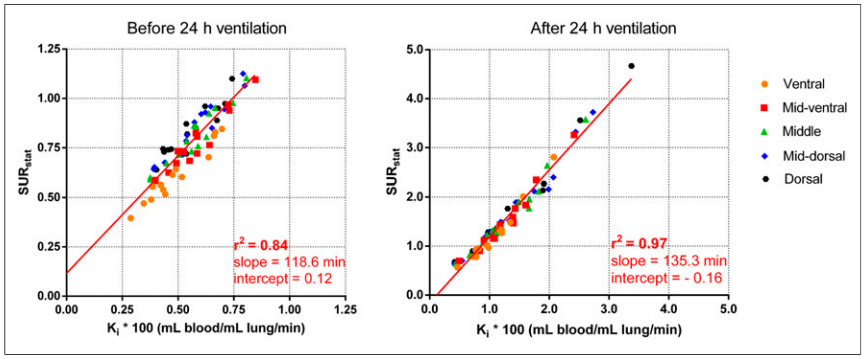

FIGURE 4. K_i–SUR_{stat} correlation obtained from PET/CT imaging data acquired before and after 24 h of mechanical ventilation and divided into 5 isogravimetric ventral (non–gravitation-dependent)–dorsal (gravitation-dependent) regions. Red lines represent linear regression lines, for which slope and intercept are specified. Note differing axis scales.

DISCUSSION

The main results of this study on an experimental model of ARDS were that, first, agreement between K_i and SUR_{stat} was stronger than that between K_i and SUV at different K_i levels; second, K_i and SUR_{stat} were strongly correlated at different levels of lung inflammation; third, the arterial input function had an essentially invariant shape across all animals and time points; and fourth, compared with K_i, SUR_{stat} and SUV tracked the same direction of

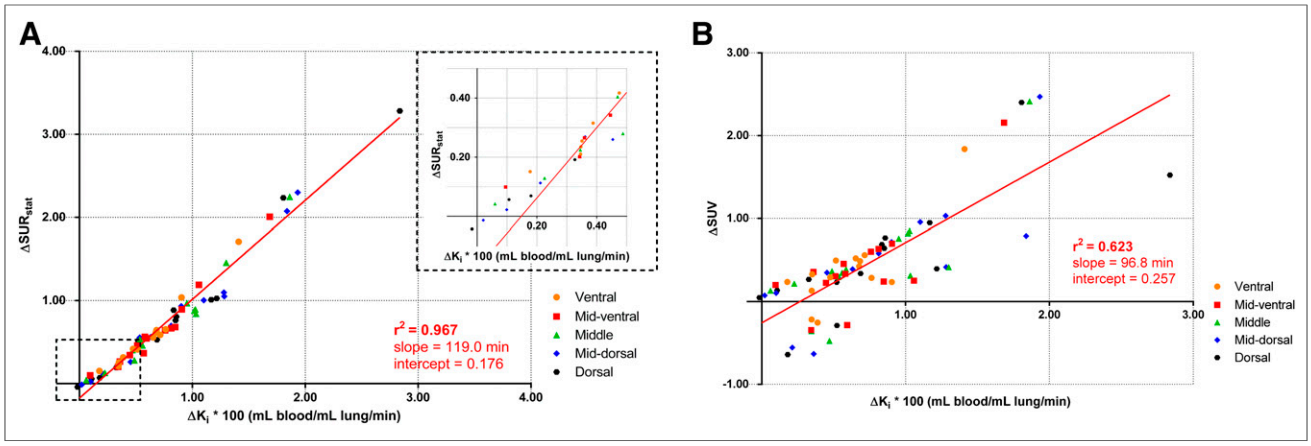

FIGURE 5. Linear correlations between regional pulmonary ΔK_i of ^{18}F-FDG and ΔSUR_{stat} (A) and between regional ΔKi and ΔSUV (B), induced by 24 h of mechanical ventilation in 14 animals and divided into 5 isogravimetric ventral (non–gravitation-dependent)–dorsal (gravitation-dependent) regions. Red lines represent linear regression lines, for which slope and intercept are specified.

change in regional lung inflammation in 98.6% and 84.3% of measurements, respectively.

SUV is a widely used parameter for quantification of ^{18}F-FDG uptake. However, SUV is dependent on factors such as body mass, injected dose of ^{18}F-FDG, and other confounding variables (*8,9*). We found a weak K_i–SUV correlation, despite a similar weight of the pigs (35.3 ± 3.6 kg), only a small variation in the injected dose of ^{18}F-FDG (198.6 ± 42.3 MBq), and acquisition of the static PET/CT scans at a similar time after ^{18}F-FDG injection (78.4 ± 0.9 min). The K_i–SUV correlation was especially weak at low levels of lung inflammation, for which variations in body mass and injected ^{18}F-FDG dose have a comparatively high impact on SUV.

The K_i–SUR correlation was much stronger than the K_i–SUV correlation at different levels of lung inflammation. Similarly, Chen et al. showed in an experimental ARDS study on dogs that K_i, determined from compartment modeling of dynamic ^{18}F-FDG data, strongly correlated with tissue-to-plasma activity ratios (calculated from the last frame of a dynamic ^{18}F-FDG scan) whereas K_i–SUV correlation was weak (*2*).

A prerequisite for the good K_i–SUR correlation is the shape invariance of the arterial input function of ^{18}F-FDG. This shape invariance across different subjects and time points has been shown in patients with liver metastasis (*5*) and colon cancer metastatic to the liver (*10*). van den Hoff et al. showed that, when the arterial input function can additionally be described by an inverse power law, the shape invariance translates into the same exponent b but a different scale factor A in Equation 1 (*7*). As a direct consequence, the Patlak time $\theta(t)$ does not depend on the individual arterial input function but, rather, is proportional to real time t. Therefore, the Patlak time is comparable between subjects at any time point after an initial period of about 3 min (*7*). van den Hoff showed that these theoretic considerations are approximately fulfilled in measurements obtained from patients with liver metastases (*7*). The investigation of the arterial input function performed in this study demonstrates that both the shape invariance of the ^{18}F-FDG input function across different animals and imaging time points and the description of the arterial ^{18}F-FDG time–activity curve by an inverse power law are also valid in pigs with ARDS. However, the exponent of the power law seems to be notably larger in pigs than in humans (0.52 compared with 0.31). In general, a shape-invariant arterial input function (as indicated by the constant exponent) is likely a

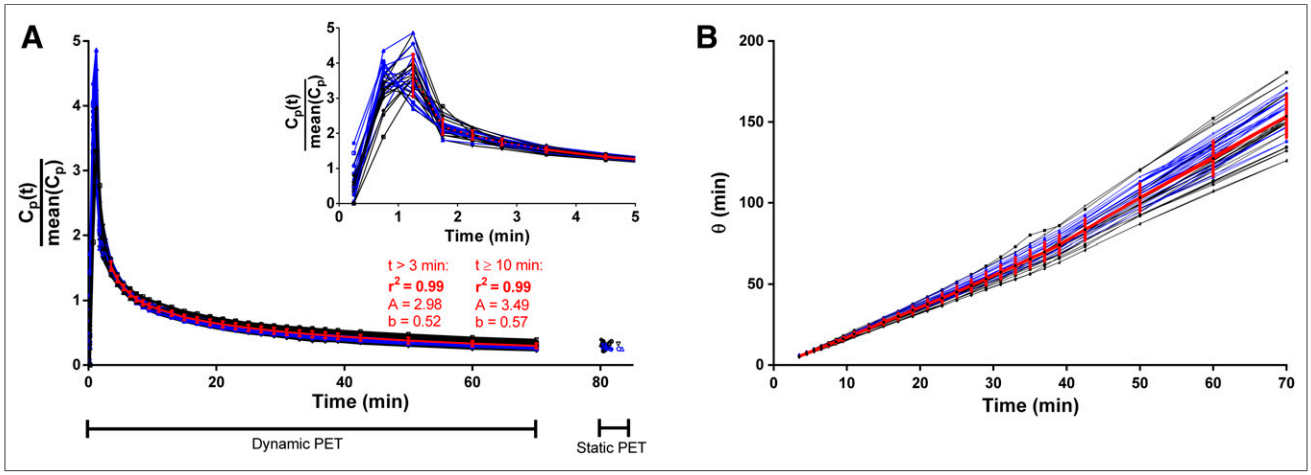

FIGURE 6. Arterial input function of ^{18}F-FDG (A) and Patlak time θ (B) at mean frame time points of dynamic PET scans. Courses are shown for 14 animals before (blue) and after (black) 24 h of mechanical ventilation. Red lines and error bars represent averages and SD of each frame. In A, interpolation was performed using the following power function: $\frac{C_{p(t)}}{C_p(t)} = A \times t^{-b}$.

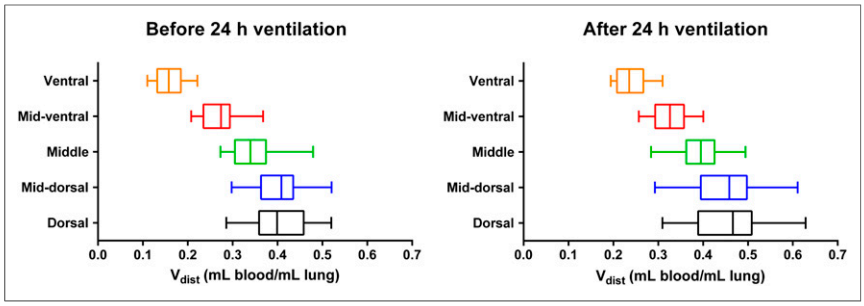

FIGURE 7. Regional V_{dist} of 14 animals before and after 24 h of mechanical ventilation.

result of a constant systemic glucose metabolism (*4*). Therefore, the differing shape of the arterial input function between pigs and humans reflects differences in systemic metabolism. However, further investigations are necessary to confirm this hypothesis.

The slightly worse K_i–SUR correlation directly after induction of lung injury than after 24 h of mechanical ventilation might be caused by the lower inflammatory values and the resultingly higher contribution of the variability of V_{dist}. The rather high intrasubject variability of V_{dist} might be explained by a substantial increase in lung perfusion from ventral to dorsal regions in supine animals (*11–13*), potentially increasing the fractional blood volume.

The 24 h period of mechanical ventilation and the associated ventilator-induced lung injury were associated with a 127.2% ± 79.4% increase in regional K_i, whereas regional V_{dist} increased by 23.2% ± 25.0%. Therefore, the contribution of the variability in regional V_{dist} was much lower after the 24 h of mechanical ventilation. This might, at least partly, explain the better K_i–SUR correlation at higher levels of pulmonary inflammation obtained after 24 h of mechanical ventilation.

The K_i–SUR correlation was performed using 2 different static PET images for SUR computation: the static PET scan measured after dynamic data acquisition (covering the whole lung, giving SUR_{stat}) and the image generated from the last frames of the dynamic PET scan (giving SUR_{dyn}). The latter was analyzed because the analysis of a static PET scan has 2 artificial sources of errors: first, there were no blood samples taken at the time point of the static PET scan. Instead, the measured arterial input function was extrapolated to this time point. Second, because of the different FOV, the image data had to be coregistered to the corresponding dynamic PET scan. Both aspects introduce an additional small error, which would not be present in a study designed accordingly. Therefore, the accuracy that can be expected when K_i is replaced by SUR is given by the results for the generated static image (SUR_{dyn}), not by the measured static image (SUR_{stat}).

A limitation of the current study is the lack of blood samples at the time point of the static whole-lung PET scan. A second limitation is the low number of investigated subjects. Further investigations with a larger sample size have to be performed before these results can be transferred to patient investigations.

CONCLUSION

In this model of experimental ARDS, the SUR analysis provided an alternative to dynamic PET scanning and Patlak modeling of the K_i of ^{18}F-FDG, allowing the assessment of inflammation of whole lungs, repeated measurements within the period of the ^{18}F-FDG decay, and faster data acquisition.

DISCLOSURE

No potential conflict of interest relevant to this article was reported.

ACKNOWLEDGMENTS

We thank Susanne Henninger Abreu, Gabriele Kotzerke, Kathrin Rosenow, and Michael Andreeff for their valuable support during the experiments.

KEY POINTS

QUESTION: Can static ^{18}F-FDG PET/CT and analysis of SUV or SUR_{stat} be used as an alternative to Patlak K_i values derived from dynamic ^{18}F-FDG PET/CT for quantification of regional lung inflammation in experimental ARDS in pigs?

PERTINENT FINDINGS: An experimental study on 14 anesthetized pigs with ARDS revealed a weaker K_i–SUV and a strong K_i–SUR correlation at 2 separate imaging time points. The good K_i–SUR_{stat} correlation can be explained by the shape invariance of the arterial input function of ^{18}F-FDG across all animals and time points.

IMPLICATIONS FOR PATIENT CARE: The findings suggest that SUR_{stat} derived from static ^{18}F-FDG PET/CT provides an alternative to dynamic ^{18}F-FDG PET/CT and Patlak K_i analysis, allowing the assessment of inflammation of whole lungs, repeated measurements within the period of ^{18}F-FDG decay, and faster data acquisition.

REFERENCES

1. Bellani G, Laffey JG, Pham T, et al. Epidemiology, patterns of care, and mortality for patients with acute respiratory distress syndrome in intensive care units in 50 countries. *JAMA*. 2016;315:788–800.
2. Chen DL, Mintun MA, Schuster DP. Comparison of methods to quantitate ^{18}F-FDG uptake with PET during experimental acute lung injury. *J Nucl Med*. 2004; 45:1583–1590.
3. Musch G, Venegas JG, Bellani G, et al. Regional gas exchange and cellular metabolic activity in ventilator-induced lung injury. *Anesthesiology*. 2007;106:723–735.
4. Paquet N, Albert A, Foidart J, Hustinx R. Within-patient variability of ^{18}F-FDG: standardized uptake values in normal tissues. *J Nucl Med*. 2004;45:784–788.
5. van den Hoff J, Oehme L, Schramm G, et al. The PET-derived tumor-to-blood standard uptake ratio (SUR) is superior to tumor SUV as a surrogate parameter of the metabolic rate of FDG. *EJNMMI Res*. 2013;3:77.
6. Hofheinz F, Hoff J, Steffen IG, et al. Comparative evaluation of SUV, tumor-to-blood standard uptake ratio (SUR), and dual time point measurements for assessment of the metabolic uptake rate in FDG PET. *EJNMMI Res*. 2016;6:53.
7. van den Hoff J, Lougovski A, Schramm G, et al. Correction of scan time dependence of standard uptake values in oncological PET. *EJNMMI Res*. 2014;4:18.
8. Carlier T, Bailly C. State-of-the-art and recent advances in quantification for therapeutic follow-up in oncology using PET. *Front Med (Lausanne)*. 2015;2:18.
9. Chen DL, Cheriyan J, Chilvers ER, et al. Quantification of lung PET images: challenges and opportunities. *J Nucl Med*. 2017;58:201–207.
10. Graham MM, Peterson LM, Hayward RM. Comparison of simplified quantitative analyses of FDG uptake. *Nucl Med Biol*. 2000;27:647–655.
11. Braune A, Scharffenberg M, Naumann A, Bluth T, de Abreu MG, Kotzerke J. Comparison of ^{68}Ga- and fluorescence-labeled microspheres for measurement of relative pulmonary perfusion in anesthetized pigs. *Nuklearmedizin*. 2018;57:100–107.
12. Glenny RW, Lamm WJ, Albert RK, Robertson HT. Gravity is a minor determinant of pulmonary blood flow distribution. *J Appl Physiol*. 1991;71:620–629.
13. Walther SM, Domino KB, Glenny RW, Hlastala MP. Pulmonary blood flow distribution in sheep: effects of anesthesia, mechanical ventilation, and change in posture. *Anesthesiology*. 1997;87:335–342.